Linear and Second-Order Pressure Effects in Velocity Centrifugation of Random Coil Polymers. Polystyrene in Cyclohexane

J. J. H. Mulderije

Gorlaeus Laboratories, Department of Physical Chemistry, State University of Leiden, 2300 RA Leiden, The Netherlands. *Received October 15, 1980*

ABSTRACT: A new method of reading schlieren pictures of narrow boundaries and handling data obtained from sedimentation velocity experiments on polymers of narrow molecular weight distribution is described. It allows determination of the sedimentation coefficient (s) and the coefficients for the linear (μ_1) and the second-order (μ_2) pressure dependences of s, with decreasing accuracy in the order given. The necessity of establishing the zero time of sedimentation is avoided. The method was tested on five polystyrenes in the Θ solvent cyclohexane. In the power series expansion of s^{-1} with respect to the pressure, μ_1 was found to increase linearly with the product of concentration and molecular weight. This increase was attended by a rapid decrease of μ_2. The concentration dependence of the pressure effect has been interpreted as an effect of the pressure on the thermodynamic interaction. The linear pressure dependence of the coefficient for the concentration dependence of the friction coefficient could be correlated with the linear temperature dependence by means of the pressure dependence of the Θ temperature. A value for $d\Theta/dp$ was derived about twice as large as was calculated from data independent of analytical centrifugation. More detailed conclusions are given at the end of the paper.

1. Introduction

Among the complications that up to the present have prevented the sedimentation velocity method from becoming a reliable means for analyzing molecular size distributions are those resulting from the hydrostatic pressure. During their migration through the cell, particles traverse a pressure gradient which at a rotor speed of 1000 rev/s may create 250 atm near the cell bottom. Here the sedimentation velocity in nonaqueous solutions will be 10–25% smaller than without compression. In the centrifugation of a polydisperse mixture with a continuous size distribution each surface at right angles to the direction of sedimentation within the gradient zone is the boundary for one of the macromolecular components, and it is the distance which each boundary travels within the same period of time under varying conditions of pressure and concentration that must be related to the sedimentation coefficient under standard conditions, that is, at 1 atm and infinite dilution. Since the resolution of a sedimentation process is proportional to the rotor speed, a high speed is preferable. Accordingly, a large pressure effect must be admitted and properly taken into account.

It has become common practice to neglect the effect of the pressure on the thermodynamic interaction and to restrict the consideration to the pressure dependence of the viscosity (η_1) and density (ρ_1) of the solvent and that of the partial specific volume ($\bar{v}_2$) of the solute. This accounts for a pressure effect which is independent of molecular weight and concentration.

For some polymer–solvent mixtures numerical data for the pressure dependence of η_1, ρ_1, and $\bar{v}_2$ are available in the literature.[1-3] For other systems it will be necessary to determine the pressure dependence of s, making use of the ultracentrifuge itself.

In this paper a new procedure for working out sedimentation velocity experiments on narrow-distribution polymers is presented. It should furnish meaningful data about the second-order pressure effect, besides more accurate values for the sedimentation coefficient and the coefficient for the linear pressure dependence.

2. Studies of the Pressure Effect Performed So Far

To date in sedimentation analyses of molecular size distributions the pressure effect has been described in terms of the simple relation

$$s^p(c) = s^0(c)(1 - \mu p) \tag{1}$$

in which $s^p(c)$ is the sedimentation coefficient at the hydrostatic pressure p and concentration c.

For pressures beyond the range where $\mu p \ll 1$ holds, the correction applied by eq 1 is too large. Nonetheless it has been preferably used in the theory of pressure-dependent sedimentation[4-6] and distribution analysis[7-9] because the resulting equations are more tractable than those obtained by substituting other relations.

For various polymer–solvent systems numerical values for μ, defined by (1), have been determined by fitting a second-degree polynomial to coordinates (r_i, t_i) of boundary positions recorded for the standard cell.[10-13] This was done by minimizing the variance

$$\sigma^2 = n^{-1}\sum_{i=1}^{n} R_i^2 \tag{2}$$

with

$$R_i = \ln (r_i/r_0) - \omega^2 s^0(c_0)(t_i - t_0) + \tfrac{1}{2}K\omega^2 s^0(c_0)(t_i - t_0)(r_i^2/r_0^2 - 1) \tag{3}$$

Here

$$K = \{m_1(1 + 2k'c_0) - k'c_0\}/(1 + k'c_0) \tag{4a}$$

$$s^0(c_0) = s^0(0)/(1 + k'c_0) \tag{4b}$$

$$m_1 = \tfrac{1}{2}\mu\rho_1\omega^1 r_0^2 \tag{4c}$$

r_0 is the distance of the meniscus from the axis of rotation, ω is the angular speed of the rotor, c_0 is the initial concentration, t_0 is the zero time of sedimentation, k' is the coefficient for the linear concentration dependence of s^{-1}, m_1 is the dimensionless parameter for the pressure dependence, and ρ_1 is the solvent density.

The combination of results obtained by the centrifugation of solutions of different concentration yields k' by using (4b). Then, for each concentration a value for μ is found from K and k' by using (4a) and (4c).

Billick[14] preferred a second-degree polynomial in $(t_i - t_0)$ rather than (3). He treated r_0 as a free parameter and took t_0 at the moment when the rotor reached $^2/_3$ of its stationary speed.

Results have been reported which are inconsistent with eq 1. Closs et al.[13] concluded that μ for the Θ systems

0024-9297/82/2215-0506$01.25/0

poly(methyl methacrylate)–1-chlorobutane at 35 °C and polystyrene–cyclohexane (PS–CH) at 34 °C is concentration dependent. They also reported a decrease of μ with increasing ω. With respect to PS–CH and PS in toluene, in Billick's work, too, a variation of μ with ω may be noticed.[14] A significant variation with concentration, however, cannot be discerned among the random errors.

A dependence of μ on the concentration, as found by Closs, means that the concentration effect is pressure dependent. This may be due to an effect of the pressure on the thermodynamic interaction. When this is true, then for a fixed concentration a dependence on the molecular weight should also exist. Abe et al.[12] studied five narrow-distribution samples of poly(α-methylstyrene) in the Θ solvent cyclohexane. Since the ranges of concentration were short, a significant variation in μ with concentration did not show up in their results. On the other hand, the range of M was wide, being a factor 29. In spite of this, a definite variation of μ with M at constant concentration was not demonstrated.

The decrease of μ with increasing ω means that for higher pressures the pressure effect is smaller than given by eq 1. This decrease showed up in experiments with boundary positions in the range $0 < r - r_0 \lesssim 0.8$ cm. For enhanced resolution in distribution analyses one may wish to extend the measurement of boundary coordinates to $r - r_0 = 1.1$ cm under conditions of high rotor speed. Obviously then, a term for the nonlinear pressure effect should be added to eq. 1. (A nonlinear effect is envisaged much larger than the systematic error introduced by neglecting the fact that for a system containing components of different compressibility the local volume flow is not rigorously zero. This is a condition for validity of the Lamm equation.)

Determination of also the second-order pressure dependence, using eq 2 and 3, would require the introduction of an additional term containing a fourth unknown parameter. We will show that it is possible to handle data using second-degree polynomials containing three unknown parameters, including the coefficient for the nonlinear pressure effect. The time t_0 will be eliminated from the equations, while r_0 is read from the photographic plate.

The Θ system PS–CH will be used for demonstration of the new approach. The dependence of the linear pressure effect on M and c will be studied as well as the magnitude of the second-order pressure effect.

3. Material Coefficients

At low polymer concentration, s can be factorized as follows:

$$s = m(1 - \bar{v}_2\rho)/\eta_1[f](1 + kw) \tag{5}$$

m is the mass of the molecule, $[f]$ is the intrinsic friction coefficient at infinite dilution, ρ is the density of the solution, k is the coefficient for the linear concentration dependence of the friction coefficient, and w is the weight fraction of polymer. $[f]$ and k depend on m and, for linear chain molecules under Θ conditions, are proportional to $m^{1/2}$.

The density of the dilute solution varies with the concentration in accordance with

$$\rho = \rho_1 + (1 - \bar{v}_2\rho_1)c \tag{6}$$

where c is the polymer concentration in weight/volume. Generally all quantities in eq 5 and 6 will be pressure dependent but m and w. Substituting (6) in (5) we obtain

$$s = m\frac{1 - \bar{v}_2\rho_1}{\eta_1}\frac{1}{[f](1 + kw)}(1 - \bar{v}_2c) \tag{7}$$

In the experiments to be discussed, the volume fraction of polymer, $\bar{v}_2c$, was smaller than 0.006. So, within a particular sedimentation process we may neglect the variation in s that results from the variation in $\bar{v}_2c$ due to the radial dilution and the compression.

For describing the pressure dependence we prefer a power series expansion of s^{-1} to an expansion of s because the former has a smaller value for the coefficient of the square term.

The pressure dependence of the first fraction in (7) is independent of particle size and concentration. We expand as follows:

$$\eta_1 = \eta_1^0(1 + \lambda_1 p + \lambda_2 p^2 + \ldots) \tag{8}$$

$$\rho_1 = \rho_1^0(1 + \kappa_1 p + \kappa_2 p^2 + \ldots) \tag{9}$$

$$\bar{v}_2 = \bar{v}_2^0(1 - \chi_1 p + \chi_2 p^2 + \ldots) \tag{10}$$

It follows from these equations that

$$\frac{\eta_1}{1 - \bar{v}_2\rho_1} = \frac{\eta_1^0}{1 - \bar{v}_2^0\rho_1^0}(1 + \nu_1 p + \nu_2 p^2 + \ldots) \tag{11}$$

in which

$$\nu_1 = \lambda_1 + \frac{\bar{v}_2^0\rho_1^0}{1 - \bar{v}_2^0\rho_1^0}(\kappa_1 - \chi_1) \tag{12a}$$

$$\nu_2 = \lambda_2 + \frac{\bar{v}_2^0\rho_1^0}{1 - \bar{v}_2^0\rho_1^0}\{(\kappa_1 - \chi_1)\lambda_1 - \kappa_1\chi_1 + \kappa_2 + \chi_2\} + \left(\frac{\bar{v}_2^0\rho_1^0}{1 - \bar{v}_2^0\rho_1^0}\right)^2(\kappa_1 - \chi_1)^2 \tag{12b}$$

The expression for ν_1 has been given by several authors.[15-17]

For a few solvents the pressure coefficients of η_1 and ρ_1 are known and have been tabulated.[1,2] The small pressure dependence of $\bar{v}_2$, too, has been determined for a number of polymer–solvent systems.[3] For other systems it can be estimated.[2]

We will include expansions that allow for an effect of the pressure on $[f]$ and k. Therefore

$$[f] = [f]^0(1 + \delta_1 p + \delta_2 p^2 + \ldots) \tag{13}$$

$$k = k^0(1 + \epsilon_1 p + \epsilon_2 p^2 + \ldots) \tag{14}$$

Omission of the square terms seems justified only after the linear terms have been found to be much smaller than unity.

Multiplying (11) and (13), we find it convenient to define coefficients $\mu_1(0)$ and $\mu_2(0)$, which represent the complete pressure effect in the limit at infinite dilution:

$$s^p(0) = s^0(0)/\{1 + \mu_1(0)p + \mu_2(0)p^2 + \ldots\} \tag{15}$$

Here

$$s^0(0) = m(1 - \bar{v}_2^0\rho_1^0)/\eta_1^0[f]^0 \tag{16}$$

and

$$\mu_1(0) = \nu_1 + \delta_1 \tag{17a}$$

$$\mu_2(0) = \nu_2 + \nu_1\delta_1 + \delta_2 \tag{17b}$$

From (7) and (15) we have

$$s^p(w) = s^0(0)/(1 + kw)\{1 + \mu_1(0)p + \mu_2(0)p^2 + \ldots\} \tag{18}$$

Finally, we define all-inclusive coefficients μ_1 and μ_2, which refer to the pressure effect at the concentration w.

After substitution of (14) in (18), multiplication, and extraction of a factor $1 + k^0w$, we obtain

$$s^p(w) = s^0(w)/(1 + \mu_1 p + \mu_2 p^2 + \ldots) \tag{19}$$

Here

$$s^0(w) = s^0(0)/(1 + k^0 w) \tag{20}$$

and

$$\mu_1(w) = \mu_1(0) + \frac{k^0 w}{1 + k^0 w}\epsilon_1 \tag{21a}$$

$$\mu_2(w) = \mu_2(0) + \frac{k^0 w}{1 + k^0 w}\{\mu_1(0)\epsilon_1 + \epsilon_2\} \tag{21b}$$

Our objective is the determination of $s^0(w)$, $\mu_1(w)$, and $\mu_2(w)$.

Next, our interest will concern the difference $\mu_1(0) - \nu_1$ for the effect of p on $[f]$ and the difference $\mu_1(w) - \mu_1(0)$ for the effect of p on k.

In appreciating experimental results it will be found useful to consider also an average coefficient $\bar{\mu}^p(w)$ defined by

$$s^p(w) = s^0(w)/\{1 + \bar{\mu}^p(w)p\} \tag{22a}$$

$\bar{\mu}^p(w)$ is related to μ_1 and μ_2 by

$$\bar{\mu}^p(w) = \mu_1(w) + \mu_2(w)p \tag{22b}$$

Since $\bar{\mu}^p$ is the slope of a chord to the function $1/s^p(w)$ vs. p, the reliability of observed values for $\bar{\mu}^p$ will be larger than for μ_1.

4. Numerical Values for ν_1 and ν_2 for PS in CH from External Sources

The literature has not yet agreed upon the significance of a concentration-dependent pressure effect for the PS–CH system, nor for any other. It is important, therefore, to know reliable reference values for the coefficients for the linear and second-order pressure effects, which should be found when the pressure dependence of $[f]$ and k is too small to be detected.

Since the buoyancy factor for PS in CH is not very small, the increase in the solvent viscosity causes the greater part of the total pressure effect (eq 12). Until recently, only an unreliable value was available for λ_1 of cyclohexane. It was estimated by Baldwin and Van Holde[1] from a single experimental datum taken from Bridgman.[18] Occasionally satisfaction has been expressed because of rough agreement obtained between the value calculated accordingly for ν_1 and observed values for $\mu_1(w)$.[8,11,13,14] This satisfaction has no ground, however, because the estimate was incorrect as may be seen in Figure 1.

Bridgman studied pure liquids at temperatures of 30 and 75 °C. He published smoothed values for η/η^0 at pressure intervals of 500 kg/cm^2. Since CH at 30 °C solidifies at about 500 kg/cm^2, only a single value for η/η^0 was listed. From this, Baldwin and Van Holde derived 1.7×10^{-9} cm^2/dyn for the apparent coefficient $(\eta/\eta^0 - 1)/p$. They supposed it to hold true approximately for 200 kg/cm^2. Other authors took the same value to appreciate coefficients established for atmospheric pressure!

A more reliable estimate is made from Bridgman's data by drawing a line through the single point for 30 °C parallel to the curve drawn to extrapolate the data for 75 °C to zero pressure. The fallibility of projecting an apparent coefficient on the ordinate is accentuated by plotting the data using the function $\ln(\eta/\eta^0)/p$ in the same figure. Both plots should yield the same intercept.

The value thus found still seems to be too high when compared with the results of Collings and McLaughlin.[19] The latter are not very different from those by Kuss.[20]

The following data were used to calculate expected values for ν_1 and ν_2 (T = 34.5 °C): $\{\lambda_1 = (1.27 \pm 0.05) \times 10^{-9}$ cm^2/dyn, $\lambda_2 = (0.44 \mp 0.06) \times 10^{-18}$ (cm^2/dyn)$^2\}$;[19] $\{\kappa_1$

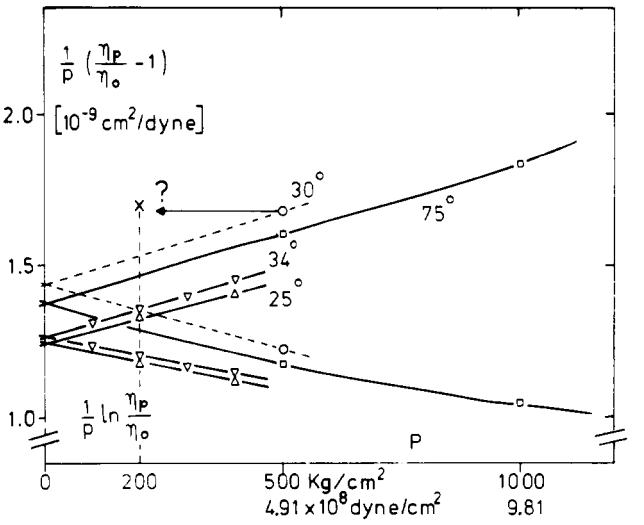

Figure 1. Apparent coefficients for the pressure dependence of the viscosity of cyclohexane from data by different authors: (○) (30 °C) and (□) (75 °C), Bridgman (1926); (▽) (34 °C), Collings and McLaughlin (1970); (△) (25 °C), Kuss (1978); (×) quotation by Baldwin and Van Holde; see text.

$= (0.124 \pm 0.001) \times 10^{-9}$ cm^2/dyn, $\kappa_2 = (-0.068 \mp 0.005) \times 10^{-18}$ (cm^2/dyn)$^2\}$;[21,22] $\{\chi_1 = (0.029 \pm 0.005) \times 10^{-9}$ cm^2/dyn, χ_2 is negligible$\}$;[3] $\rho_1^0 = 0.7648$ g/mL (private measurement); $\bar{v}_2^0 = 0.9431$ mL/g.[23] Substitution of these values in eq 12 gives

$$\nu_1 = (1.51 \pm 0.06) \times 10^{-9} \text{ cm}^2/\text{dyn} \tag{23a}$$

$$\nu_2 = (0.62 \mp 0.07) \times 10^{-18} \text{ (cm}^2/\text{dyn)}^2 \tag{23b}$$

In order to know the magnitude of the terms for the linear and second-order pressure effects, we choose $p = 215 \times 10^6$ dyn/cm^2, which is the pressure in CH at 1000 rev/s at $x = 0.4$ with $r_0 = 5.95$ cm (eq 31). This gives $\nu_1 p = 0.324 \pm 0.013$ and $\nu_2 p^2 = 0.028 \mp 0.003$.

In similarity to (22b) we have

$$\bar{\nu}^p = \nu_1 + \nu_2 p \tag{24}$$

For the pressure mentioned above, the $\bar{\nu}^p$ going with ν_1 and ν_2 from (23) is

$$\bar{\nu}^{215} = (1.64 \pm 0.04) \times 10^{-9} \text{ cm}^2/\text{dyn} \tag{25}$$

5. From Schlieren Exposures to Coefficients for the Pressure Effect

The position of the sharp boundary that would appear in the absence of diffusion is given by the root second moment of the cell coordinate ($\langle r^2\rangle^{1/2}$) with respect to the boundary gradient on the condition that the solute concentration at the meniscus has vanished and a plateau region is present.[24] This also holds with the pressure effect, provided the theoretical difference between the plateau concentrations at the leading end of the gradient and $\langle r^2\rangle^{1/2}$ is negligibly small.

Since the evaluation of $\langle r^2\rangle^{1/2}$ takes up much time and major errors proceed from the ends of the boundary where the gradient curve is flat, we worked in a different way. On inspection of the schlieren pattern of a narrow gradient (Figure 2) it is seen that points on the steep sides are measured with greater accuracy than the tails and the top. Hence for a narrow boundary the determination of a point on the midline, which keeps equal distances to the steep sections (measured in a direction parallel to the base line), is likely to entail smaller random errors. This point should be taken at the level of the center of gravity of the surface enclosed by the gradient curve and the base line for the following reasons. The distance of the center of gravity

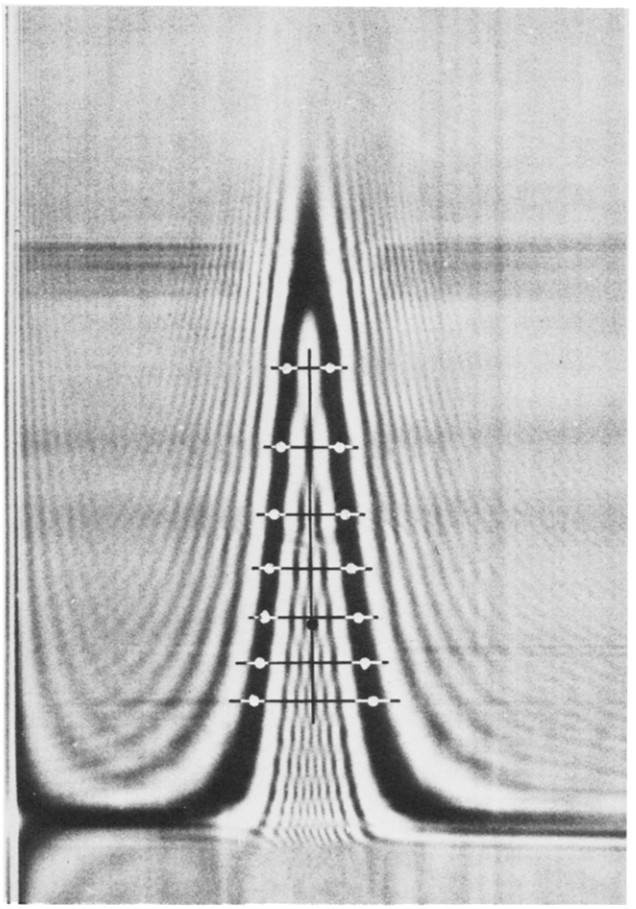

Figure 2. Determination of the median section and an approximate center of gravity using the interference pattern inside the schlieren image of the refractive index gradient. PS-19 in cyclohexane, concentration 0.4% (w/w). Rotor speed 59 780 rev/min. Cell thickness 12 mm. Exit window 1° negative wedge.

from the rotor axis equals the first moment $\langle r \rangle$ of the cell coordinate with respect to the boundary gradient. For narrow boundaries $\langle r \rangle$ differs insignificantly from $\langle r^2 \rangle^{1/2}$. The center of gravity is on the midline when this line is straight, either vertical or skew. If skewness is due to a systematic error in the depiction of the gradient, then still the error in the position of the center of gravity will be smaller than the error in the position of the maximum by a factor $1/2\sqrt{2}$, which is the ratio of the ordinates of these points for a Gaussian function. For a narrow boundary and with a proper adjustment of the camera lens, the skewness of the midline can only be small, so a rigorous determination of the height of the center of gravity will not be required.

For a gradient of Gaussian shape at a distance of 65 mm (cell center) to the rotor axis it can be shown that

$$\langle r^2 \rangle^{1/2} - \langle r \rangle = 0.0014(d_{1/2})^2 \text{ mm} \tag{26}$$

$d_{1/2}$ is the width of the gradient at half top height and is expressed in millimeters.

The correction is very small, but it is a systematic one. Since the reading of points of the steep sides of narrow-boundary gradients can be reproduced with a precision of a few thousandths of a millimeter, it may be worthwhile to apply a correction for boundaries for which $d_{1/2} \gtrsim 2$ mm.

Designating the equivalent boundary position on schlieren exposure j as r_j, we should correlate positions r_j and times t_j ($j = 1, 2, ..., n$) to determine local values of s_j^{-1} defined by

$$s_j^{-1} = \omega^2 r_j (\mathrm{d}r/\mathrm{d}t)_j^{-1} \tag{27}$$

The following equation was used to find intercepts using the method of least squares

$$\frac{1}{\omega^2 s_{ij}} \equiv \frac{t_i - t_j}{\ln (r_i/r_j)} = \frac{1}{\omega^2 s_j} + b_{1j}(r_i^2 - r_j^2) + b_{2j}(r_1^2 - r_j^2)^2 \tag{28}$$

$$(i, j = 1, 2, ..., n; \qquad i \neq j; \qquad |(r_i^2 - r_j^2)/r_0^2| < \zeta)$$

Pattern j is combined with other patterns that have boundaries lying within a reduced distance ζ (= 0.25, e.g.) from the reference point. In succession all patterns are taken as the reference pattern. The coefficients b_{1j} and b_{2j} vanish if s is independent of pressure and concentration. In that case $s_{ij} = s_j$.

Use of eq 28 is preferable to the use of $\ln (r_i/r_j)/(t_i - t_j)$ because when the pressure effect is large, the former shows less curvature in the curve fitted to the plotted data.

Indicating the running character of the boundary by an asterisk, we must prepare eq 18 for substitution of data $((\omega^2 s_*)^{-1}, x_*)$, with $x_* \equiv r_*^2/r_0^2 - 1$. We write

$$(\omega^2 s_*)^{-1} = \{\omega^2 s^0(0)\}^{-1}\{1 + k(p_*)w_*\}\{1 + \mu_1(0)p_* + \mu_2(0)p_*^2\} \tag{29}$$

We have to express p_* and w_* in x_*. The hydrostatic pressure follows from the equation

$$\mathrm{d}p_*/\mathrm{d}r_* = \rho_1(p_*)\omega^2 r_* \tag{30}$$

The solvent density should be substituted from (9). Integration, application of the boundary condition $p_* = 0$ ($r_* = r_0$), introduction of x_*, and expansion of the resulting expression yield

$$p_* = \tfrac{1}{2}\rho_1{}^0\omega^2 r_0^2 x_* + \tfrac{1}{8}\kappa_1(\rho_1{}^0\omega^2 r_0^2 x_*)^2 + ... \tag{31}$$

At the bottom of the useful column length and at 1000 rev/s the contribution by the second term will not be larger than 2%. Nonetheless, the resulting correction in s may be larger than the margin of experimental errors.

Substituting (31) in (18), we write

$$\frac{1}{\omega^2 s_*} = \frac{1}{\omega^2 s^0(0)}(1 + \gamma_*\vartheta_*)(1 + m_1 x_* + m_2 x_*^2 + ...) \tag{32}$$

in which dimensionless variables are used as follows:

$$\gamma_* \equiv k(p_*)w_0 \tag{33a}$$

$$\vartheta_* \equiv w(x_*)/w_0 \tag{33b}$$

$$m_1 \equiv \tfrac{1}{2}\mu_1(0)\rho_1{}^0\omega^2 r_0^2 \tag{34a}$$

$$m_2 \equiv \tfrac{1}{4}\{\mu_2(0) + \tfrac{1}{2}\kappa_1\mu_1(0)\}(\rho_1{}^0\omega^2 r_0^2)^2 \tag{34b}$$

w_0 is the initial concentration of the homogeneous solution.

Substituting for p in (14), we write the expansion for

$$\gamma_* = \gamma^0(1 + h_1 x_* + h_2 x_*^2 + ...) \tag{35}$$

in which

$$\gamma^0 \equiv k^0 w_0 \tag{36a}$$

$$h_1 \equiv \tfrac{1}{2}\epsilon_1\rho_1{}^0\omega^2 r_0^2 \tag{36b}$$

$$h_2 \equiv \tfrac{1}{4}(\epsilon_2 + \tfrac{1}{2}\kappa_1\epsilon_1)(\rho_1{}^0\omega^2 r_0^2)^2 \tag{36c}$$

Since $\vartheta_* = 1$ ($x_* = 0$), the extrapolation of $(\omega^2 s_*)^{-1}$ to the meniscus yields $\{\omega^2 s^0(w_0)\}^{-1} = (1 + \gamma^0)/\omega^2 s^0(0)$.

We propose to evaluate $\mu_1(w_0)$ and $\mu_2(w_0)$ (eq 21) by fitting a second-degree polynomial in x_* to the set of values for $(\omega^2 s_*)^{-1}$, after a correction for the small difference in concentration effect resulting from the difference between the local concentration $w(x_*)$ and w_0.

We may explain the new approach by first finding coefficients l_1 and l_2 that would be obtained if the relation $\gamma(x_*)$ were known and the exact correction factor $(1 + \gamma_*)/(1 + \gamma_*\vartheta_*)$ could be applied. Multiplying eq 32 by this factor and fitting the polynomial, numerical values will result for l_1 and l_2, defined by

$$\frac{1 + \gamma_*}{1 + \gamma_*\vartheta_*}\frac{1}{\omega^2 s_*} = \frac{1}{\omega^2 s^0(w_0)}\{1 + l_1 x_* + l_2 x_*^2 + ...\} \quad (37)$$

On the grounds of eq 32, 35, 20, and 36a, these coefficients are composed as follows:

$$l_1 = m_1 + \frac{\gamma^0}{1 + \gamma^0}h_1 \quad (38a)$$

$$l_2 = m_2 + \frac{\gamma^0}{1 + \gamma^0}(m_1 h_1 + h_2) \quad (38b)$$

They are related to $\mu_1(w_0)$ and $\mu_2(w_0)$ by

$$l_1 = \tfrac{1}{2}\mu_1(w_0)\rho_1{}^0\omega^2 r_0{}^2 \quad (39a)$$

$$l_2 = \tfrac{1}{4}\{\mu_2(w_0) + \tfrac{1}{2}\kappa_1\mu_1(w_0)\}(\rho_1{}^0\omega^2 r_0{}^2)^2 \quad (39b)$$

These relations result from eq 38, 34, 36a,b, and 21a for l_1 and from eq 38, 34, 36a,c and 21a,b for l_2.

The approach (37) is invited by the particular relationship of ϑ_* with x_*. It is proven in Appendix 1[25] that for practical values of x_* and m_1, viz., $0 < x_* \lesssim 0.4$ and $0 \leq m_1 \lesssim 1$, for $|h_1| < 1$, and for small square terms, viz., $|m_2 x_*^2| \ll 1$ and $|h_2 x_*^2| \ll 1$, the following expression for ϑ_* will approximate the exact value to within 1%, provided $0 \leq \gamma^0 \lesssim 0.25$:

$$\vartheta_* = \frac{(1 + m_1 x_* + m_2 x_*^2 + ...)(1 + \gamma_*)}{(1 + x_*)(1 + \gamma^0)} = \frac{1 + l_1 x_* + l_2 x_*^2 + ...}{1 + x_*} \quad (40)$$

Since the numerator equals the expansion in (37), an iterative fitting of a polynomial, making use of eq 37 and 40 with initial value $\vartheta_* = 1$, would rapidly yield stationary values for l_1 and l_2. (Dishon et al.[6] erred in their conclusion that in a system with concentration effect, ϑ_* is not explicitly dependent on γ^0; see Appendix 1.[25])

The complete correction suggested in (37) is not feasible, however, because $\gamma(x_*)$ is unknown. What can be procured from some additional experimentation is k^0 $(=\gamma^0/w_0)$.[26] For this reason we multiply (32) by $(1 + \gamma^0)/(1 + \gamma^0\vartheta_*')$ instead, with ϑ_*' to follow. We thus obtain

$$\frac{1 + \gamma^0}{1 + \gamma^0\vartheta_*'}\frac{1}{\omega^2 s_*} = \frac{1}{\omega^2 s^0(w_0)}\frac{1 + \gamma_*\vartheta_*}{1 + \gamma^0\vartheta_*'}(1 + m_1 x_* + m_2 x_*^2 + ...) \quad (41)$$

By expanding the right-hand member, we will get a form

$$\frac{1 + \gamma^0}{1 + \gamma^0\vartheta_*'}\frac{1}{\omega^2 s_*} = \frac{1}{\omega^2 s^0(w_0)}(1 + l_1' x_* + l_2' x_*^2 + ...) \quad (42)$$

For ϑ_*' we take in similarity to (40)

$$\vartheta_*' = \frac{1 + l_1' x_* + l_2' x_*^2 + ...}{1 + x_*} \quad (43)$$

The relations of l_1' and l_2' to l_1 and l_2 are found by substituting for γ_*, ϑ_*', and ϑ_* from eq 35, 43, and the right-hand member of (40) in eq 41, followed by expansion in powers of x_*. From identification of the coefficients of corresponding terms of the resulting expression and eq 42, we obtain after rearrangement and some reduction, making use of eq 38

$$l_1' = l_1 \quad (44a)$$

$$l_2' = l_2 - \frac{\gamma^0}{(1 + \gamma^0)(1 + 2\gamma^0)}h_1(1 - l_1) \quad (44b)$$

The difference between l_2' and l_2 is small. It will vanish both when the effect of the pressure on the concentration dependence of the friction coefficient is negligible ($h_1 = 0$) and when there is a strong pressure effect ($l_1 \to 1$).

Using once more (38a) and taking l_2 explicit, we have

$$l_1 = l_1' \quad (45a)$$

$$l_2 = l_2' + \frac{(l_1' - m_1)(1 - l_1')}{1 + 2\gamma^0} \quad (45b)$$

in which $m_1 = \lim_{w_0 \to 0} l_1 = \lim_{w_0 \to 0} l_1'$.

Since the difference of the correction factor applied in (41) with unity is small, a polynomial of the second degree in x_* fitting the set of coordinates $(1/\omega^2 s_*, x_*)$ will yield $s^0(w_0)$ and initial values for l_1' and l_2'. Then γ^0 is introduced and stationary values are obtained for l_1' and l_2' after two or three iterations using eq 42 and 43.

Centrifugation of a given solution will yield a value for l_1 for the concentration used. Centrifuging the same polymer at different concentrations enables us to extrapolate l_1 to zero concentration to obtain m_1. Then l_2 can be evaluated for each centrifugation using eq 45b. Finally $\mu_1(w_0)$ and $\mu_2(w_0)$ follow by means of eq 39.

Inspection of data in the literature about the pressure dependence of the viscosity of pure liquids shows that m_1 at the maximum speed of 1000 rev/s for aluminum rotors will not be larger than unity. Consequently, for a given x_* the correction factor will be closer to unity in measure as the rotor speed is higher and the pressure effect is larger.

6. Experiments and Calculations

Polymers. The specifications of five narrow-distribution polystyrenes, purchased from Pressure Chemical Co., are in Table I. $\bar{M}_w$ and heteromolecularity ratios are those given by the manufacturer, except for PS-19. From the intrinsic viscosity and the elution time at gel permeation chromatography a value 200 000 was found to be too high.

Table I
Specification of Polystyrenes

designation	batch no.[a]	$\bar{M}_w \times 10^{-3}$	$\bar{M}_w/\bar{M}_n$
PS-10	4a	98	≤1.06
PS-16	1a	160	≤1.06
PS-19	1c	190	≤1.06
PS-41	3a	411	≤1.06
PS-86	6a	860	≤1.15

[a] Batch number of manufacturer.

Solvent. CH of analytical reagent grade was supplied by Merck. Since the nominal water content was 0.01% or less, no attempt was made to thoroughly dry the solvent. It has been reported that this gives no differences in the results.[9]

Solutions were prepared and prewarmed cells filled according to good standard practice. An easy redissolution of sediment pellets and homogenization of the solution was achieved by revolving the cell for several hours at 1 rev/s using a homemade turntable with a horizontal axis of rotation and placed in a container of warm air. The shortest edge of the cell cavity was oriented parallel to the axis so that the air bubble jumped from corner to corner, thus keeping the solution in steady agitation.

Cells. Aluminum centerpieces of 12-, 6-, or 3-mm thickness were used according to concentration and molecular weight. The window toward the light source was sapphire, and the one toward

the camera lens was quartz and was either plane or a 1° negative wedge.

Centrifugation. A Spinco E analytical ultracentrifuge was used. Experiments were carried out at the maximum allowed speed for aluminum rotors (59780 rev/min). It was not considered useful to use also lower speeds for the following reason. The linear pressure effect is evaluated from the change in s with x as given approximately by the relation

$$(\mu_1)_{obsd} \approx -\frac{2}{\rho\omega^2 r_0^2} \lim_{x\to 0} \left(\frac{1}{s}\frac{ds}{dx}\right)_{obsd} \quad (46)$$

If the random error in ds/dx were independent of rotor speed, the probable error in $(\mu_1)_{obsd}$ would already decrease inversely with ω^2. However, the precision in locating boundary positions increases with rotor speed because a higher sedimentation velocity gives the boundary less time to broaden as a result of diffusion. The random error in $(\mu_1)_{obsd}$ may therefore be expected to decrease more rapidly than in inverse proportion to ω^2. Consequently, any large difference between the coefficients $(\mu_1)_{obsd}$ evaluated at a lower and at a higher speed is not likely to be significant on the grounds of a greatly increased error margin for the run at lower speed (cf. results by Billick[14]).

In order to offset in time the adiabatic temperature decrease of 0.8 °C, the initial temperature was set 0.6 °C above the equilibrium temperature of 34.5 °C. Additional heat was supplied during the accelaration. Eighteen photos were taken, early time intervals being somewhat shorter than later ones. Sedimentation was continued until the boundary had traveled about 11 mm.

For each M a few additional experiments of shorter duration were made for providing k^0. For details see ref 26.

The camera lens was adjusted as recommended by Svensson.[27] A plane (the virtual object plane) situated two-thirds of the cell thickness from the window of light entrance, measured in the solvent-filled cell, was imaged on the plate.

The nearly uniform refractive index gradient induced in the solvent by the pressure gradient, together with the skew position of the phase edge, tends to lift the schlieren pattern off the plate. The lateral shift of the phase plate necessary to return the image is larger than the standard mounting of the plate allows of. To provide for a wider range, the phase plate holder was modified to fit a dovetail slide mounted perpendicular to the optical track. Movement along the slide was regulated by means of a dumbscrew.

Photography. Ilford G30 chromatic plates of 1.5-mm glass thickness were used. Plates 1.0 mm thick were not held tight against the bottom of the plate holder.

Reading the Plate. Within the schlieren curve of a narrow boundary an interference pattern is visible made up of several levels of short vertical fringes (Figure 2). The number of fringe levels primarily depends on the refractive index increment across the boundary. For each level the horizontal coordinates of the points of intersection of the gradient branches with a line drawn at right angles to the meniscus were read. When the base line was inclined or curved, the line of intersection was chosen parallel to the local tangent to the base line. The midpoints of the intersections on each level were plotted on widely spaced graph paper. In the vertical direction the ratio of the distances between the interference levels was copied roughly from the schlieren image, the same sequence of separations being taken for all boundary patterns of the same experiment. The points were interpolated or extrapolated to the level of $1/2\sqrt{2}$ times the height of the gradient curve or slightly higher. In case the midline was curved, a correction was estimated. This was always very small. According to the quality of the pattern, levels below about $^1/_4$ maximum height were disregarded. During an experiment the ratio of the height of the fringe levels to the top of the gradient diminishes somewhat due to the boundary broadening and the radial dilution. This causes the center of gravity to move slightly upward with respect to these levels. This calls for some care in the interpolation.

Less meticulous plate reading was required in the experiments for concentration effect because here only one parameter had to be established.

A few meniscus fringes that stood out clearly through the whole series of exposures were measured for reference purposes. They were preferred to the images of the reference holes because for reasons of symmetry the cross hairs of the microscope can be placed directly over a fringe with better reproducibility than over a one-sided edge.

Calculations were carried out at an IBM computer using a program written in Algol. The input included positions and times (r_j, t_j) of the boundaries, the position of the meniscus (r_0), the parameter γ^0, and three interval limits. The following calculations were carried out:

1. Local values for s^{-1} and their probable random errors were determined using eq 28 and the least-squares method. The limit ζ was set at 0.25. In accordance with the probable error in the ordinate each pair of coordinates was assigned a statistical weight $(r_i - r_j)^2$.

2. The errors were used to assign weight factors for a second curve fitting, viz., the regression of the intercepts with respect to x_* on the basis of eq 32. The small variation of $\gamma_*\vartheta_*$ with x_* was neglected thereby. Again the boundaries for $x_* > 0.25$ were not included in this computation. From this a definite meniscus value for s^{-1} followed along with numerical values for the coefficients of x_* and x_*^2. These were initial values for l_1' and l_2'.

3. First values for ϑ_* were computed by substituting these values in (43). Then γ^0 was taken up from the input data and the correction factor applied in (41) calculated. The regression of the corrected and weighted intercepts to x_* was then repeated, while the constant term of the polynomial was fixed at the output value of operation 2 and an upper limit of $x_* < 0.4$ was imposed. This procedure was repeated twice to improve on l_1' and l_2'.

In desk work $\mu_1(w_0)$ and $\mu_2(w_0)$ were calculated from l_1' and l_2' using eq 45 and 39. m_1 was determined by plotting l_1 against $\gamma^0/(1 + \gamma^0)$ (eq 38a) and by extrapolating to $\gamma^0 = 0$.

7. Results

Results are listed in Table II. The entries for each w_0 are averages for 2, 3, or 4 experiments. In addition, the averages of the absolute values of the residues are given. For $w_0 \to 0$ it is the standard deviation. Figure 3 illustrates operation 1 of the calculations. Only half the number of intercepts made for one experiment are shown. Figure 4 shows the rapid increase of s_*^{-1} with x_*. The data for $x_* \leq 0.25$ were used to determine the intercepts which equal $1/s^0(w_0)$.

The expedient of finding the midline has reduced the random error in $1/s^0(w_0)$, as demonstrated by its smooth variation with w_0 (Figure 5). Values for k^0 may be derived from the slopes $(=k^0/s^0(0))$. Since these values are required in the analysis of experiments but are not available until after the experiments for a given M are concluded, they were determined in advance by a different method.[26] In this method the boundary distances for two solutions of different w_0, traveled in equal periods of time, are plotted on different axes (x_{w_1} vs. x_{w_2}). The deviation of the initial slope from unity is a measure for k^0. The results of both methods agree well (Figure 6). The straight line through 0 represents the relation

$$k_\Theta{}^0 = (3.15 \pm 0.15) \times 10^{13}\{s^0(0)\}_\Theta \text{ g/g} \quad (47)$$

A marked increase of μ_1 with w_0 is found. This confirms the findings by Closs.[13] Although it is accompanied by a decrease of μ_2, an increase is still present in the average coefficient $\bar{\mu}^{215}$ for the larger M.

For PS-16 at small w_0, μ_1 has fallen too low when compared with the next smaller and larger M. As a consequence μ_2 is too large. For PS-10 a significant variation of μ_1 with w_0 is not apparent. These less consistent results can be partly explained from the fact that for smaller M and w_0 the random error in locating the center of gravity of a boundary is increased as a result of the greater boundary spreading and the larger inclination of the phase plate. The latter magnifies not only the gradient peak but also any slope or curvature of the base line.

For PS-19, -41, and -86 the average μ_1 values for each w_0 have been plotted vs. $w_0/(1 + k^0 w_0)$ in Figure 7 (eq 21a).

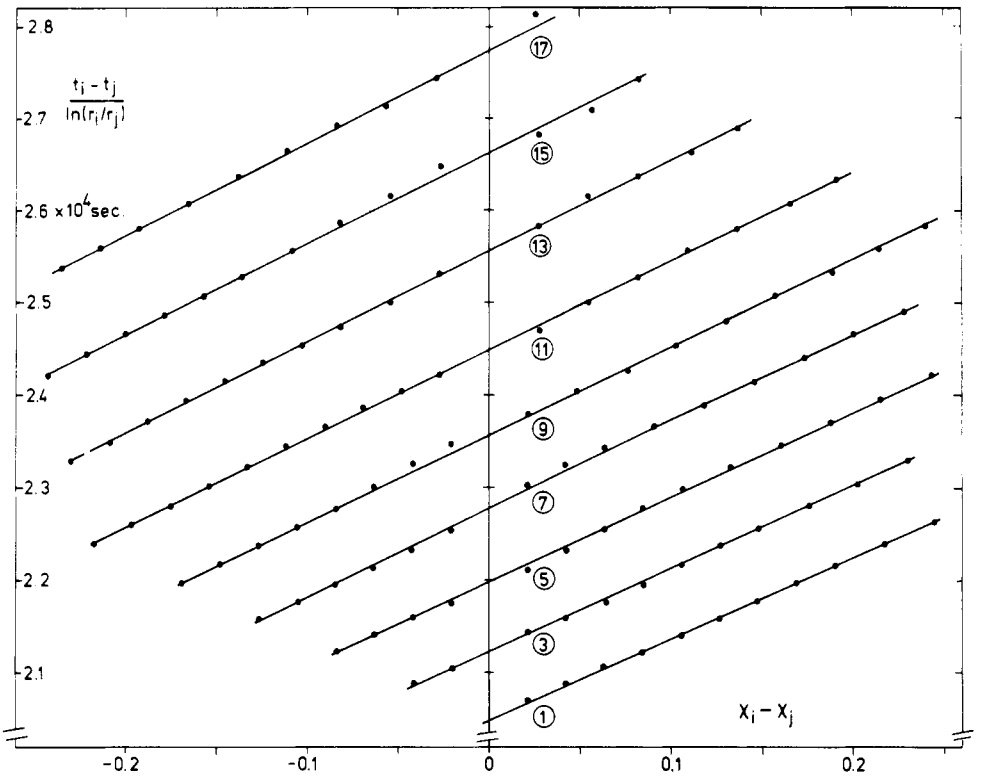

Figure 3. Illustration of operation 1 of the calculations. The intercepts equal $(\omega^2 s_j)^{-1}$ (eq 28). Only the inter(extra)polations of odd number are shown. PS-86 in CH, 0.24% (w/w). T = 34.5 °C. Rotor speed 59 780 rev/min.

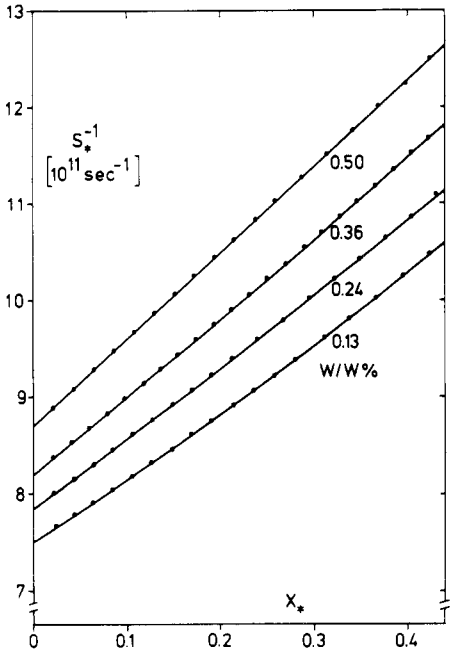

Figure 4. Rapid increase of s_*^{-1} with x_* under conditions of large pressure effect. PS-86 in CH. Rotor speed 59 780 rev/min.

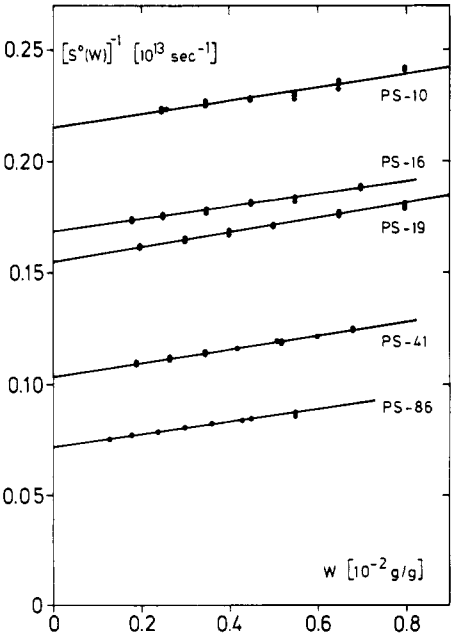

Figure 5. $\{s^0(w_0)\}^{-1}$ vs. w_0 at the Θ point. Slopes equal $[k^0/s^0(0)]_\Theta$ and are independent of particle size. PS–CH, T = 34.5 °C.

The dot and the bar on the vertical axis denote ν_1 and its error margin as given by (23a). The intercepts for PS-41 and -86 are outside this interval. However, their reliability is questionable in view of Figure 8, which shows a similar plot for $\bar{\mu}^{215}$ in accordance with eq 22b and 21a,b. Here no intercept is outside the error margin for $\bar{\nu}^{215}$ given by (25). Since the reliability of observed values for $\bar{\mu}^{215}$ is larger than for μ_1, we conclude that the experiments have demonstrated no dependence of $[f]$ on p. In contrast to this, the increase of μ_1 with w_0 is evident. On the grounds of eq 14 and 21a $(\partial k/\partial p)_T{}^0/k^0 = \epsilon_1$. Taking the slopes from Figure 7 and values for k^0 as following from (47), we find $\epsilon_1 = 1.6 \times 10^{-9}$, 2.6×10^{-9}, and 3.2×10^{-9} cm²/dyn for PS-19, -41, and -86, respectively. These values are even larger than ν_1 and are in sharp contrast to the small values for $(\partial[f]/\partial p)_T{}^0/[f]^0 = \delta_1$.

We next will examine whether these results can be explained from an effect of the pressure on the thermodynamic interaction.

8. Correlating the Pressure and Temperature Dependence of $[f]$ and k for a Θ Solution

Separation of structural and thermodynamic factors in $[f]$ is achieved in the familiar expressions

$$[f] = [f]_\Theta \alpha_f \tag{48a}$$

$$[f]_\Theta = B\langle l_0^2\rangle^{1/2} \tag{48b}$$

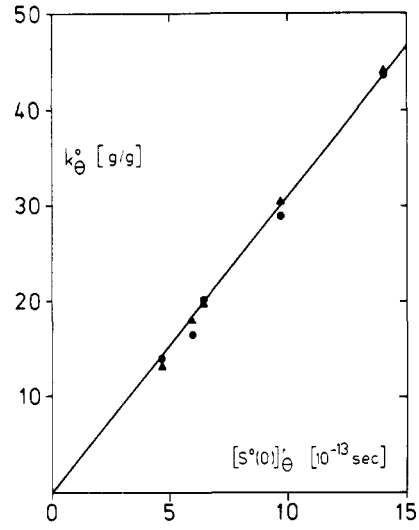

Figure 6. Plot showing consistency of the coefficients of concentration dependence for s^{-1} obtained by two methods: (●) from $1/s^0(w_0)$ vs w_0; (▲) from x_{w_1} vs. x_{w_2}. PS–CH, T = 34.5 °C.

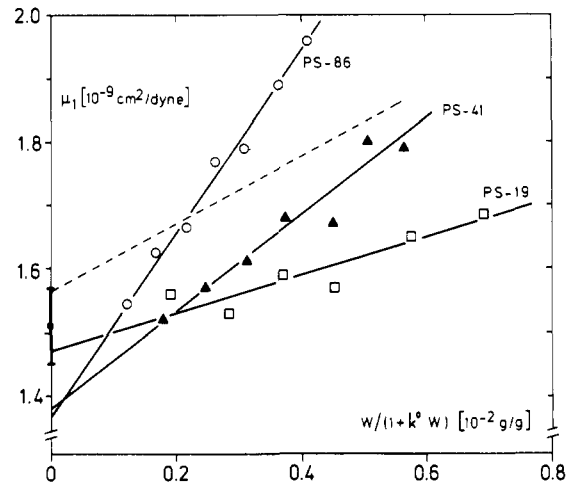

Figure 7. Coefficients $\mu_1(w_0)$ plotted in accordance with eq 21a. Bar on vertical axis denotes error margin of calculated value for $\mu_1(0)$ using data from independent sources and assuming $[f]$ to be independent of the pressure. Broken line is discussed in section 9. PS–CH, T = 34.5 °C.

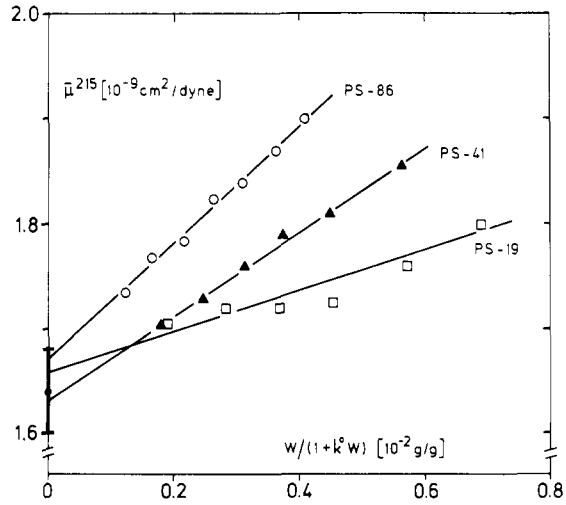

Figure 8. Apparent values for the coefficient of pressure dependence of s^{-1} for $p = 215 \times 10^6$ dyn/cm². For the bar on the vertical axis see the caption to Figure 7.

α_f is the linear expansion factor for friction in translation and is unity at $T = \Theta$, $\langle l_0^2 \rangle$ is the mean-square end-to-end distance of the linear unperturbed cain, and B is a numerical factor independent of M and the nature of the polymer and solvent.

Equations 48a and 48b are asymptotically valid for distributions of many segments. Their application is not restricted to atmospheric pressure, so we may consider the variation of B, $\langle l_0^2 \rangle$, and α_f with p. $[f]$ is the ensemble average of a large number of values for f/η_0, each applying to a particular spatial distribution of the segments. For each distribution, f/η_0 is determined completely by geometrical factors. On the $\Theta(p)$ line the excluded volume is zero and the distributions expand or contract with varying p in proportion to $\langle l_0^2 \rangle^{1/2}$. Since for similar distributions the ratios of the friction coefficients equal those of the linear dimensions, and since in (48b) the linear dimension is present as a separate factor, p and T are irrelevant variables for the value of B. On these grounds

$$\delta_1 \equiv \left(\frac{\partial \ln [f]}{\partial p}\right)_T = \frac{1}{2}\left(\frac{\partial \ln \langle l_0^2 \rangle}{\partial p}\right)_T + \left(\frac{\partial \alpha_f}{\partial p}\right)_T \qquad (T = \Theta) \quad (49)$$

Now, let us consider the variation of some quantity ξ, relevant to chain molecules, with p and T in the vicinity of the Θ point. The total derivative of ξ with respect to p along the $\Theta(p)$ line is related to the partial derivatives as follows:

$$\left(\frac{d\xi}{dp}\right)_\Theta = \left(\frac{\partial \xi}{\partial p}\right)_T + \left(\frac{\partial \xi}{\partial T}\right)_p \frac{d\Theta}{dp} \qquad (T = \Theta) \quad (50)$$

When ξ stands for α_f, the members of this equation are zero, because α_f is constant (=1) on the $\Theta(p)$ line. We thus have

$$\left(\frac{\partial \alpha_f}{\partial p}\right)_\Theta = -\left(\frac{\partial \alpha_f}{\partial T}\right)_p \frac{d\Theta}{dp} \qquad (51)$$

In the ultracentrifuge a wide range in T is available, whereas for variations in p one is restricted to 1–200 atm. When $d\Theta/dp$ is small, thermodynamic effects will be measured with greater reliability as a function of T rather than p.

Substitution of numerical values for $(\partial \alpha_f/\partial T)_p$ in (51) provides through (49) and (17a) a prediction of the variation of δ_1 and $\mu_1(0)$ with M. From a study of the temperature dependence of s for PS in CH in the vicinity of the Θ point we take the result[26]

$$(\partial \alpha_f/\partial T)_p = (0.87 \pm 0.04) \times 10^{-5} M^{1/2} \text{ deg}^{-1} \qquad (T = \Theta) \quad (52)$$

In Appendix 2[25] source material is discussed from which a value for $d\Theta/dp$ independent of analytical centrifugation can be derived. Data which answer the purpose best are from Saeki et al.[31] These authors measured the pressure dependence of the upper critical solution temperature for PS in CH for four molecular weights in the range 1–50 atm. When their data are extrapolated to infinite M, one obtains

$$d\Theta/dp = -(0.8 \pm 0.1) \text{ °C/100 atm} \quad (53)$$

A similar value is deduced from the ratio of the variations in the total volume and the enthalpy that occur upon dissolving amorphous PS in CH (−1.0 °C/100 atm).[25]

Relying on (52) and (53), we have

$$(\partial \alpha_f/\partial p)_T = (0.7 \pm 0.1) \times 10^{-13} M^{1/2} \text{ cm}^2/\text{dyn} \qquad (T = \Theta) \quad (54)$$

It would follow from (54), (49), and (17a) that $\mu_1(0)$ for PS-19 is 0.03×10^{-9} cm²/dyn larger than ν_1, and for PS-86

Table II
Sedimentation Coefficients, Coefficients for the Linear and the Second-Order Pressure Dependences of s^{-1}, and Apparent Coefficients across the Full Pressure Range Used ((0–215) × 10^6 dyn/cm^2)[a]

w_0, wt %	$s^0(w_0) \times 10^{13}$, s	$\mu_1 \times 10^9$, cm^2/dyn	$\mu_2 \times 10^{18}$, (cm^2/dyn)^2	$\bar{\mu}^{215} \times 10^9$, cm^2/dyn	$\mu_1{}^T \times 10^2$, deg^{-1}
		PS-10			
0	4.64 ± 0.04[b]	(1.40 ∓ 0.08)[b]		1.62 ± 0.05[b]	not used
0.25	4.48 ± 0.01	1.45 ∓ 0.02	0.9 ± 0.2	1.64 ± 0.03	
0.35	4.42 ± 0.02	1.36 ∓ 0.01	1.7 ± 0.1	1.73 ± 0.00	
0.45	4.39 ± 0.01	1.55 ∓ 0.04	1.0 ± 0.1	1.77 ± 0.03	
0.55	4.38 ± 0.01	1.56 ∓ 0.06	1.0 ± 0.3	1.78 ± 0.01	
0.65	4.27 ± 0.02	1.61 ∓ 0.04	0.7 ± 0.1	1.76 ± 0.02	
0.80	4.14 ± 0.00	1.56 ∓ 0.02	1.0 ± 0.1	1.77 ± 0.01	
		PS-16			
0	5.93 ± 0.03[b]	(1.15 ∓ 0.08)[b]		1.76 ± 0.03[b]	not used
0.18	5.76 ± 0.01	1.25 ∓ 0.02	2.4 ± 0.1	1.77 ± 0.03	
0.25	5.71 ± 0.01	1.36 ∓ 0.01	1.6 ± 0.1	1.70 ± 0.03	
0.35	5.64 ± 0.01	1.43 ∓ 0.05	1.3 ± 0.2	1.69 ± 0.02	
0.45	5.54 ± 0.01	1.44 ∓ 0.01	1.1 ± 0.1	1.68 ± 0.01	
0.55	5.47 ± 0.01	1.57 ∓ 0.01	0.9 ± 0.1	1.76 ± 0.02	
0.70	5.33 ± 0.02	1.62 ∓ 0.06	0.7 ± 0.2	1.77 ± 0.01	
		PS-19			
0	6.44 ± 0.03[b]	1.47 ∓ 0.04[b]		1.66 ± 0.02[b]	1.43 ± 0.04[b]
0.20	6.19 ± 0.01	1.56 ∓ 0.01	0.64 ± 0.04	1.70 ± 0.02	1.15
0.30	6.08 ± 0.02	1.53 ∓ 0.06	0.9 ± 0.2	1.72 ± 0.01	1.04
0.40	5.96 ± 0.03	1.59 ∓ 0.01	0.60 ± 0.04	1.72 ± 0.02	0.95
0.50	5.85 ± 0.01	1.57 ∓ 0.02	0.71 ± 0.09	1.72 ± 0.00	0.80
0.65	5.69 ± 0.03	1.65 ∓ 0.03	0.50 ± 0.09	1.76 ± 0.02	0.61
0.80	5.55 ± 0.01	1.69 ∓0.04	0.52 ± 0.15	1.80 ± 0.01	0.48
		PS-41			
0	9.68 ± 0.08[b]	1.38 ∓ 0.04[b]		1.64 ± 0.02[b]	1.30 ± 0.02[b]
0.19	9.19 ± 0.04	1.52 ∓ 0.01	0.88 ± 0.08	1.70 ± 0.03	0.79
0.265	8.99 ± 0.02	1.57 ∓ 0.01	0.75 ± 0.10	1.73 ± 0.01	0.59
0.345	8.82 ± 0.03	1.61 ∓ 0.01	0.70 ± 0.02	1.76 ± 0.01	0.39
0.42	8.67 ± 0.02	1.66 ∓ 0.03	0.63 ± 0.01	1.79 ± 0.03	0.20
0.52	8.43 ± 0.02	1.67 ∓ 0.04	0.66 ± 0.18	1.81 ± 0.01	−0.01
0.60	8.26 ± 0.01	1.80 ∓ 0.03	0.20 ± 0.13	1.84 ± 0.01	−0.22
0.68	8.08 ± 0.03	1.79 ∓ 0.01	0.28 ± 0.05	1.85 ± 0.01	−0.43
		PS-86			
0	14.05 ± 0.08[b]	1.37 ∓ 0.03[b]		1.67 ± 0.015[b]	1.06 ± 0.03[b]
0.13	13.30 ± 0.00	1.545 ∓ 0.005	0.89 ± 0.03	1.735 ± 0.005	0.32
0.18	13.01 ± 0.01	1.625 ∓ 0.015	0.66 ± 0.02	1.77 ± 0.01	0.05
0.24	12.70 ± 0.00	1.67 ∓ 0.03	0.54 ± 0.14	1.78 ± 0.02	−0.21
0.30	12.46 ± 0.01	1.77 ∓ 0.01	0.26 ± 0.02	1.825 ± 0.005	−0.49
0.36	12.13 ± 0.03	1.79 ∓ 0.00	0.23 ± 0.01	1.84 ± 0.00	−0.77
0.44	11.85 ± 0.04	1.89 ∓ 0.02	−0.07 ± 0.04	1.87 ± 0.03	−1.14
0.50	11.57 ± 0.08	1.96 ∓ 0.01	−0.28 ± 0.02	1.90 ± 0.01	−1.46

[a] Error margins defined in the text. In last column coefficients for the linear temperature dependence of $s^0(w_0)$ (section 8). Polystyrene-cyclohexane (T = 34.5 °C). [b] Extrapolated values.

0.065 × 10^{-9} cm^2/dyn. In contrast to these positive values, the intercepts in Figure 7 suggest small negative contributions.

The pressure dependence of $\langle l_0^2 \rangle$ is unknown. Presumably it is small and even negligible compared with ν_1 (eq 23a), when note is taken of the magnitude of the corresponding temperature coefficients

$$\frac{1}{2}\left(\frac{\partial}{\partial T} \ln \langle l_0^2 \rangle\right)_p = (2 \pm 1) \times 10^{-4} \text{ deg}^{-1} \quad \text{(ref 32)} \tag{55}$$

$$\left(\frac{\partial}{\partial T} \ln \frac{1 - \bar{V}_2\rho_1}{\eta_1}\right)_p = (1.77 \pm 0.01) \times 10^{-2} \text{ deg}^{-1} \quad (T = 34.5 \text{ °C, ref 26}) \tag{56}$$

If pressure dependence of $\langle l_0^2 \rangle$ is to make good for the difference between the calculated and observed values for $\mu_1(0)$, then the coefficients must be negative. We will return to this point in the discussion of the pressure dependence of k.

Only binary interaction is involved in the value of k. At small Reynolds numbers the hydrodynamic interaction between two equal chain molecules does not affect their relative position,[33] so the distribution function for the mass centers of two chains migrating under an external force depends on the thermodynamic interaction in the same manner as it does at mechanical rest. Along the $\Theta(p)$ line the value of k_Θ will vary no more than corresponds with the cubic expansion or contraction of the random-flight distributions of the interacting molecules. Besides, the volume change of the solution should be considered.

Since a small concentration effect is proportional to a hydrodynamic volume, V_e, of the chain molecules, it is useful to express w in terms of the volume fraction of impermeable equivalent spheres, Φ

$$kw = k_\varphi\Phi = k_\varphi n V_e \tag{57}$$

k_φ and V_e will vary with p, T, M, and the nature of the polymer and solvent.

Substituting $w\rho N_A/M$ for the number density of spheres n, we have

$$k = k_\varphi \rho N_A V_e / M \tag{58}$$

In Pyun and Fixman's satisfying theory[34,35] for k, the radius R_e of the equivalent sphere is related to $[f]$ according to $R_e = [f]/6\pi$. In this model R_e is independent of the hydrodynamic interaction between two chains. In the two-parameter theory for the real chain polymer the intramolecular and intermolecular thermodynamic interaction is governed by the excluded volume variable z. Since z is zero on the $\Theta(p)$ line, $k/\rho\langle l_0^2\rangle^{3/2}$ is invariable along this line.

Taken rigorously, the concept of equivalence requires that the sphere be defined as an interaction equivalent sphere. At constant $\langle l_0^2\rangle$ and z, the radius of this sphere varies to such an extent that the friction coefficient of two spheres in hydrodynamic interaction equals the friction coefficient of two chain molecules with the same center-to-center distance. Thus the radius will be dependent on z and $\langle l_0^2\rangle^{1/2}/R_{12}$. An average value for this radius will result from a spatial averaging with respect to $\bar{R}_{12}$, which is necessary to obtain k.

In this view the intermolecular interaction expresses itself also in the radius of the equivalent sphere. This leaves the conclusion about $k/\rho\langle l_0^2\rangle^{3/2}$ unchanged, however.

Avoiding the use of the friction-equivalent sphere, we consider the following expression for k:

$$k = Q(z)\rho N_A \langle l_0^2\rangle^{3/2}/M \tag{59}$$

$Q(z)$ is a numerical function of z.

It follows from eq 14 and 59 that

$$\epsilon_1 \equiv \left(\frac{\partial \ln k}{\partial p}\right)_T = \frac{\mathrm{d} \ln Q}{\mathrm{d}z}\left(\frac{\partial z}{\partial p}\right)_T + \left(\frac{\partial \ln \rho}{\partial p}\right)_T + \frac{3}{2}\left(\frac{\partial \ln \langle l_0^2\rangle}{\partial p}\right)_T \tag{60}$$

Since for our PS samples ϵ_1 is larger than 1.5×10^{-9} cm^2/dyn, we will neglect the last term of (60) on the same grounds as previously $^1/_2\partial \ln \langle l_0^2\rangle/\partial p$ with respect to ν_1.

We thus consider k/ρ as constant along the $\Theta(p)$ line and then have in view of (50)

$$\left(\frac{\partial(k/\rho)}{\partial p}\right)_T = -\left(\frac{\partial(k/\rho)}{\partial T}\right)_p \frac{\mathrm{d}\Theta}{\mathrm{d}p} \qquad (T = \Theta) \tag{61}$$

z in the two-parameter theory for the real chain polymer is

$$z = \{3/(2\pi\langle l_0^2\rangle)\}^{3/2}\beta n^2 \tag{62}$$

β is the effective volume excluded to one segment of the equivalent statistical chain by the presence of another one. n is the number of segments.

From (61) and (62) we obtain, considering that $\beta = 0$ on the Θ line,

$$\left(\frac{\partial(k/\rho)}{\partial p}\right)_T = -\left(\frac{3}{2\pi}\right)^{3/2}\frac{\mathrm{d}Q}{\mathrm{d}z}N_A\left(\frac{\partial\beta}{\partial T}\right)_p \frac{n^2}{M}\frac{\mathrm{d}\Theta}{\mathrm{d}p} \sim M\frac{\mathrm{d}\Theta}{\mathrm{d}p} \qquad (p \to 0,\ T = \Theta) \tag{63}$$

in which the pressure dependence of $\langle l_0^2\rangle$ has been neglected.

The slopes from Figure 7 have been corrected for the compressibility of the solution using κ_1 and the density ρ_1^0 stated in section 4, and k_Θ^0 given by (53). They have been plotted in Figure 9. In accordance with eq 63 proportionality with M is demonstrated:

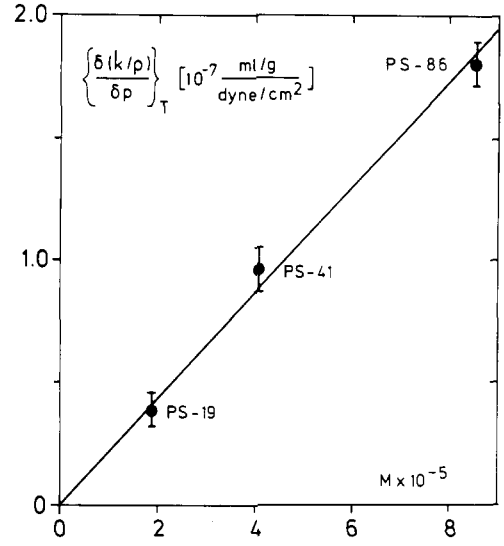

Figure 9. Pressure dependence of k/ρ at the Θ temperature increases in proportion to M. PS–CH, T = 34.5 °C.

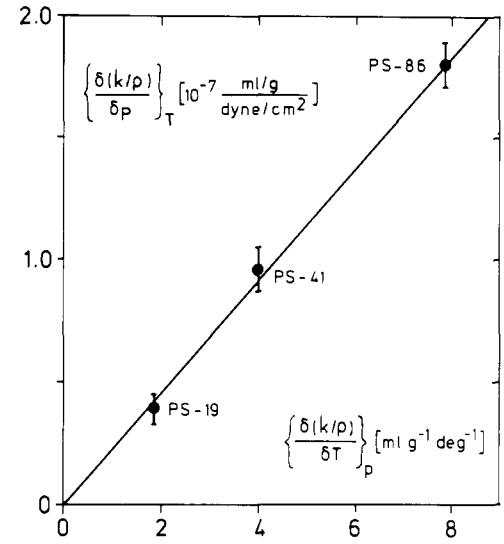

Figure 10. Ratio of the pressure and the temperature dependence of k/ρ at the Θ temperature is independent of M and equals $-\mathrm{d}\Theta/\mathrm{d}p$. PS-CH, 34.5 °C.

$$\{\partial(k/\rho)/\partial p\}_T = (2.1 \pm 0.1) \times 10^{-13} M \text{ cm}^5/(\text{g·dyn}) \qquad (T = \Theta) \tag{64}$$

We use eq 61 to evaluate $\mathrm{d}\Theta/\mathrm{d}p$. Temperature coefficients for $s^0(w_0)$ determined in the study mentioned previously[26] are quoted in Table II. From these the following temperature derivatives for k/ρ at T = 34.5 °C are derived: $\{\partial(k/\rho)/\partial T\}_p$ = 1.86 ± 0.1, 4.0 ± 0.1, and 7.9 ± 0.1 mL g^{-1} deg^{-1} for PS-19, -41, and -86, respectively.

Figure 10 shows that the ratio of the pressure and temperature derivatives of k/ρ is the same for different M. The slope suggests that

$$\mathrm{d}\Theta/\mathrm{d}p = -(2.30 \pm 0.15)\ ^\circ\text{C}/100 \text{ atm} \tag{65}$$

This value makes quite a difference with (53). The difference is in excess of the expected value, whereas for $(\partial \ln [f]/\partial p)_T$ it was of opposite sign to the calculated effect. It follows that the origin of these differences cannot be found in the neglect of $\partial \ln \langle l_0^2\rangle/\partial p$ because if its value were significant, it would either increase or decrease both $[f]$ and k according to sign. Nonetheless, experiment and calculation agree in that the relative variation in $[f]$ is very

small compared with that in k.

We take closer view of $(\delta_1/\epsilon_1)_\Theta$, as estimated from the temperature coefficients of $[f]$ and k^0. For $M \gtrsim 10^5$ the ratio of $^1/_2(\partial \ln \langle l_0^2\rangle/T)_p$ to $(\partial\alpha_f/\partial T)_p$ is $< 10^{-1}$. Assuming that $^1/_2\,(\partial \ln \langle l_0^2\rangle/\partial p)_T$ is likewise small compared with $(\partial\alpha_f/\partial p)_T$, we have $(\mathrm{d} \ln [f]/\mathrm{d}p \approx 0$ and therefore

$$\delta_1 \approx -(\partial \ln [f]/\partial T)_p(\mathrm{d}\Theta/\mathrm{d}p) \qquad (T = \Theta) \qquad (66)$$

Neglecting in (61) the small pressure and temperature dependence of the solvent density, we have with greater reliability

$$\epsilon_1 = -(\partial \ln k^0/\partial T)_p(\mathrm{d}\Theta/\mathrm{d}p) \qquad (T = \Theta) \qquad (67)$$

with k^0 defined by (14).

From the variation of the temperature coefficients of s, listed in Table II, in combination with (47), it can be deduced that

$$(\partial \ln k^0/\partial T)_p = (15.5 \pm 1) \times 10^{-5} M^{1/2}\ \mathrm{deg}^{-1} \qquad (T = \Theta) \qquad (68)$$

It follows from (52), (66), (67), and (68) that

$$(\delta_1/\epsilon_1)_\Theta \approx (\partial \ln [f]/\partial T)_p/(\partial \ln k^0/\partial T)_p = 0.056 \pm 0.005 \qquad (69)$$

Assuming that thermodynamic effects are also dominant in the values for δ_2 and ϵ_2, we suppose $|\delta_1/\epsilon_1| \ll 1$ to be followed by $|\delta_2/\epsilon_2| \ll 1$ (eq 13 and 14). Indeed, the rapid decrease of μ_2 with increasing concentration can only be represented by a value for ϵ_2 which is large negative. A small value for $|\delta_2|$ is supported by the results for $\bar{\mu}^{215}(0)$ (Figure 8). This average coefficient shows no significant variation through the range of measured M. Besides, it is scarcely different from $\bar{\nu}^{215}$.

9. Error Sources

In view of the results a discussion of error sources is indicated.

1. *Temperature Errors.* A pulse of heat injected into the rotor under vacuum, using the heating wire at the base of the rotor, is dissipated through the rotor mass within 3 min. This was observed on the RTIC pointer. This fact, together with the measures stated in the experimental section, should ensure that a constant temperature is reached by the time the first exposure is made.

2. It was claimed at least once[37] that the *heat of compression* generated in the solution by the rotor acceleration takes many minutes to flow off into the rotor. In the opinion of the present author this time is much shorter. The differential equation for heat diffusion is readily solved for a system made up of a liquid of initial temperature T_0 enclosed between two parallel infinitely wide walls of constant temperature $T_w < T_0$. It is found that the time in which the temperature difference in the midplane falls off to e^{-1} of its initial value equals $b^2\rho C_p/\pi^2\lambda$, in which b is the distance between the cell walls and ρ, C_p, and λ are the density, specific heat, and heat conductivity for the liquid concerned. For the usual average cell width of 0.45 cm and for CH ($\rho = 0.77$ g/cm^3, $C_p = 0.44$ cal/(g·deg), $\lambda = 3.6 \times 10^{-4}$ cal/(cm·s·deg)) a characteristic time for heat dissipation of 19 s is calculated.

The authors of the paper mentioned presumably had bad luck in chosing chloroform to demonstrate the predicted temperature gradient. Many grades of chloroform are doped with ethanol to prevent oxidation. The origin of the observed refractive index gradient should therefore be found in an alcohol gradient rather than in a temperature gradient.

3. *Misadjustment of the camera lens* gives rise to a systematic difference between the first moments of the cell coordinate with respect to the real and the virtual boundary gradient. In velocity centrifugation, however, it is not the exact boundary positions which count, but the exact differences in the positions on different exposures. An error in the position which is constant on account of an invariable shape of the boundary is without effect. Now, the boundary broadening will be smaller according as M and w_0 are larger. It follows that the differential systematic error in the boundary positions and the resulting error in μ_1 must be likewise smaller. In Figure 7 the broken line represents the increase of μ_1 with w_0 for PS-86 calculated from the temperature dependence of $s^0(w_0)$ by making use of eq 52 and 68. For $\mathrm{d}\Theta/\mathrm{d}p$ the value (53) was taken. If this line gives the true increase, the observed μ_1 should approach this line to the right. In contrast to this, they keep a straight course and steadily increase their distance to the broken line. Apparently, the origin of the rapid variation of μ_1 and μ_2 with w_0 cannot be found in a small misadjustment of the camera lens.

4. *Calculated Concentration at the Equivalent Boundary Point.* For PS-86 the observed value for ϵ_1 is about 3×10^{-9} cm^2/dyn. From (36b) we have $h_1 \approx 1.7$. By substituting this value, as well as $x_* = 0.4$ and the highest used value for γ^0, 0.22, in eq 22′,[25] it is verified that the condition stated for the validity of the approximation for ϑ_* is not violated.

5. The *fluctuations in the rotor speed* are small and the period time is short compared with the time between two exposures. Their effect on the results for $s^0(w_0)$ and μ_1 will be insignificant. Moreover, it is of random character.

10. Conclusions and Final Remarks

1. By determining the center of gravity of the boundary gradient, making use of points of the steep sides of the gradient peak, the equivalent boundary position for a narrow-distribution polymer is evaluated with greater reliability than from the gradient maximum. From these boundary positions local values of s^{-1} can be calculated with precision. By extrapolation to the meniscus, $s^0(w_0)^{-1}$ is obtained without necessity to establish t_0.

2. At high rotor speeds and in nonaqueous solvents the pressure effect is nonlinear. For PS–CH and at 1000 rev/min the linear variation in s with p may reach −32% and the nonlinear variation +8%.

3. The concentration dependence of the pressure effect or, in other words, the effect of the pressure on the concentration dependence of the friction coefficient, should be interpreted as an effect of the pressure on the radial distribution function for two particles and through this on their hydrodynamic interaction.

4. The variation of ln $[f]$ with p and T is very small compared with that of ln k.

5. Near the Θ point the rate of change of k/ρ with p and T is proportional to M.

6. The ratio of these derivatives equals $-\mathrm{d}\Theta/\mathrm{d}p$. Thus we found for PS–CH $\mathrm{d}\Theta/\mathrm{d}p = -2.3$ °C/100 atm (eq 65). Other sources lead to a value −1.0 °C/100 atm (Appendix 2).[25]

We further observe that unless the pressure dependence of the thermodynamically unperturbed dimensions is very large, $(\partial[f]/\partial p)_T < 0$ in addition to $(\partial k/\partial p)_T > 0$, as suggested by our experiments, is inconsistent with the two-parameter theory for the real chain polymer.

In the analysis of molecular size distributions it is required that a pair of coefficients μ_1 and μ_2 gives an adequate correction for the pressure effect. Since errors in μ_1 and μ_2 tend to have opposite signs, this requirement can be fulfilled. In the direct expansion of s the square term must be included rather than in an expansion of s^{-1}.

Distribution analyses are performed at low concentrations. Besides, for PS–CH $\mu_1(0)$ was found to be little different from ν_1, like $\bar{\mu}^{215}$ from $\bar{\nu}^{215}$. This will be true for most polymer–solvent systems. Coefficients for the linear and second-order pressure effects may therefore be considered which do not include a pressure-dependent thermodynamic interaction or, alternatively, are given a value calculated for the weight average of $M^{1/2}$ for the distribution investigated.

A stronger effect of pressure on the excluded volume may be expected to occur for a polymer–solvent pair for which the total volume undergoes a larger change on mixing. In the event of contraction a rise in the pressure will cause the chain molecules to expand. Thus the discontinuous state of the solution with respect to the segments is diminished and a further reduction in the volume of the solution is achieved. Contraction, therefore, goes with a pressure effect which increases with M and w_0. Hence a more rapid increase of μ_1 with M and w will occur for PS in butanone than in CH. In butanone at 0.5 segment fraction of polymer, Flory and Höcker[38] observed a volume decrease 6 times larger than they found for PS in CH. However, since PS–butanone is athermal, a linkage of the pressure and temperature dependence as suggested by eq 51 and 61 cannot be made.

Acknowledgment. The author is grateful to Professor Dr. A. J. Staverman for many discussions and comments on manuscripts. Thanks are also due to Drs. A. J. H. Kemper, who prepared the major part of the Algol program.

Supplementary Material Available: Appendix 1, where eq 40 is derived, and Appendix 2, where $d\theta/dp$ (eq 53) is discussed (8 pages). Ordering information is given on any current masthead page.

References and Notes

(1) Baldwin, R. L.; van Holde, K. E. *Fortschr. Hochpolym. Forsch.* **1958**, *1*, 451, 496.
(2) Mulderije, J. J. H. Thesis, Rijksuniversiteit Leiden, 1978.
(3) Anderson, G. R. *Ark. Kemi* **1963**, *20*, 513.
(4) Fujita, H. *J. Am. Chem. Soc.* **1956**, *78*, 3598.
(5) Fujita, H. "Foundations of Ultracentrifugal Analysis"; Wiley: New York, 1975.
(6) Dishon, M.; Weiss, G. H.; Yphantis, D. A. *J. Polym. Sci., Part A-2* **1970**, *8*, 2163.
(7) Billick, I. H. *J. Polym. Sci.* **1962**, *62*, 167.
(8) Wales, M.; Rehfeld, S. J. *J. Polym. Sci.* **1962**, *62*, 179.
(9) Blair, J. E.; Williams, J. W. *J. Phys. Chem.* **1964**, *68*, 161.
(10) Cowie, J. M. G.; Bywater, S. *Polymer* **1965**, *6*, 179.
(11) Noda, I., et al. *J. Phys. Chem.* **1967**, *71*, 4048.
(12) Abe, M., et al. *Bull. Chem. Soc. Jpn.* **1968**, *41*, 2330.
(13) Closs, W. J.; Jennings, B. R.; Jerrard, H. G. *Eur. Polym. J.* **1968**, *4*, 651.
(14) Billick, I. H. *J. Phys. Chem.* **1962**, *66*, 1941.
(15) Oth, J.; Desreux, V. *Bull. Soc. Chim. Belg.* **1954**, *63*, 133.
(16) Meyerhoff, G. In "Ultracentrifugal Analysis in Theory and Experiment"; Williams, J. W., Ed.; Academic Press: New York, 1963.
(17) Elias, H. G. *Makromol. Chem.* **1959**, *24*, 30.
(18) Bridgman, P. W. *Proc. Am. Acad. Arts Sci.* **1926**, *61*, 57.
(19) Collings, A. F.; McLaughlin, E. *Trans. Faraday Soc.* **1970**, *67*, 340.
(20) Calculated from data received from Dr. E. Kuss, Institut für Erdölforschung, Hannover, West Germany.
(21) Holder, G. A.; Whally, E. *Trans. Faraday Soc.* **1962**, *58*, 2095.
(22) Kuss, E.; Taslimi, M. *Chem.-Ing.-Tech.* **1970**, *42*, 1073.
(23) Schulz, G. V.; Hoffmann, M. *Makromol. Chem.* **1957**, *23*, 220.
(24) Goldberg, R. J. *J. Phys. Chem.* **1953**, *57*, 194.
(25) See the paragraph at end of text concerning supplementary material.
(26) Mulderije, J. J. H. *Macromolecules* **1980**, *13*, 1207.
(27) Svensson, H. *Opt. Acta* **1954**, *1*, 25.
(28) Flory, P. J. "Principles of Polymer Chemistry"; Cornell University Press: Ithaca, N.Y., 1953; p 609.
(29) Kirkwood, J. G.; Riseman, J. *J. Chem. Phys.* **1948**, *16*, 565.
(30) Stockmayer, W. H.; Albrecht, A. C. *J. Polym. Sci.* **1958**, *32*, 215.
(31) Saeki, S., et al. *Polymer* **1975**, *16*, 445.
(32) Review in: Flory, P. J. "Statistical Mechanics of Chain Molecules"; Interscience: New York, 1969; Chapter 2.
(33) Oseen, C. W. "Hydrodynamik"; Akademische Verlagsgesellschaft: Leipzig, 1927; p 157.
(34) Pyun, C. W.; Fixman, M. *J. Chem. Phys.* **1964**, *41*, 937.
(35) Mulderije, J. J. H. *Macromolecules* **1980**, *13*, 1526.
(36) See: Yamakawa, H. "Modern Theory of Polymer Solutions"; Harper and Row: New York, 1971; p 84.
(37) Mijnlieff, P. F.; van Es, P.; Jaspers, W. J. M. *Recl. Trav. Chim. Pays-Bas* **1969**, *88*, 2.
(38) Flory, P. J.; Höcker, H. *Trans. Faraday Soc.* **1971**, *67*, 2258.

Screened Hydrodynamic Interactions in a Semidilute Solution of Rodlike Macromolecules

Sezar Fesciyan*,† and John S. Dahler*

Departments of Chemistry and Chemical Engineering, University of Minnesota, Minneapolis, Minnesota 55455. *Received August 26, 1981*

ABSTRACT: We have extended the theory of Doi and Edwards for a semidilute solution of rodlike molecules by including the effects of hydrodynamic interactions into the expression for the stress tensor. This is done by using the solution of the Kirkwood–Riseman equation, modified for the semidilute regime by the inclusion of a screened hydrodynamic interaction tensor, as derived by Freed and Edwards. When hydrodynamic interactions are neglected, our result for the shear dependence of the normalized viscosity reduces to the extended version of the Doi and Edwards theory due to Jain and Cohen. Inclusion of hydrodynamic interactions gives excellent agreement with experimental results.

Introduction

Kirkwood was the first to formulate a logically consistent theory of the contributions of hydrodynamic interactions to the dynamics of polymeric solutions. This theory, based on the Oseen tensor, was successfully applied to dilute solutions of rodlike molecules as early as 1950.[1] It produced significant improvements over earlier theories of rods which had ignored the hydrodynamic interactions.

There is substantial experimental and theoretical evidence that at sufficiently high concentrations screening totally obliterates the effects of hydrodynamic interactions. However, there is an intermediate range of number con-

†Present address: Department of Physics, Manhattan College, Bronx, N.Y. 10471.

0024-9297/82/2215-0517$01.25/0